PERGAMON

Scripta mater. 42 (2000) 967–973

Scripta MATERIALIA

www.elsevier.com/locate/scriptamat

COARSENING KINETICS OF δ'-Al_3Li PRECIPITATES: PHASE-FIELD SIMULATION IN 2D AND 3D

V. Vaithyanathan and L.Q. Chen

Materials Science and Engineering, Pennsylvania State University, University Park, PA 16802, USA

(Received September 6, 1999)
(Accepted in revised form December 22, 1999)

Keywords: Phase-field; Coarsening; Al-Li; Computer simulation

Introduction

Precipitation takes place during aging of a quenched homogeneous alloy within a two-phase field. The main process which occurs during the late stages of a precipitation reaction is particle coarsening, during which, larger particles grow while smaller particles dissolve in the matrix, driven by total interfacial energy reduction. Coarsening is an important issue in controlling the thermal stability of two-phase alloys against degradation of mechanical properties at high temperatures.

The first formal theory of coarsening was LSW theory [1,2], which predicts that cube of average particle size vs. time has a linear dependence and normalized particle size distributions (PSDs) are invariant with time. LSW theory assumes that precipitates have spherical shapes and the number of particles is small so that the typical inter-particle distance is large compared to average precipitate size. Therefore, in principle, LSW theory is applicable only to systems with a very low volume fraction. Volume fractions of precipitates in real systems are always finite, and the spatial correlations and diffusional interactions between precipitates become increasingly important as the volume fraction increases. There have been many attempts to modify LSW theory by taking into account the effect of volume fraction [3,4]. Recently, Marsh and Glicksman even proposed a coarsening theory for the entire volume fraction range [5]. Due to complexity of coarsening processes, particularly at high volume fractions, current analytical theories are still unable to satisfactorily explain the experimentally measured volume-fraction dependences of both PSD and coarsening rate constant simultaneously.

To reduce the number of approximations and relax some of the assumptions made in analytical theories, there has been an increasing number of numerical computational studies of coarsening processes [6,7,8,9]. Most of the existing simulation studies were performed in 2D and only a few of them in 3D [10,11,12]. For the particular case of Al-Li alloys, recently, we employed the microscopic field model to study the morphological evolution and coarsening kinetics of δ' precipitates [13]. Even though computer simulations using microscopic field approach were performed in projected 2D systems, many aspects of the simulation results including volume fraction dependence of precipitate morphology and coarsening rates show at least qualitative agreement with existing experimental measurements. The main purpose of this paper is to compare the similarities and differences between coarsening kinetics obtained in 2D and 3D computer simulations. For this purpose, we chose a 20% volume fraction system and employed the continuum diffuse-interface phase-field approach which has been extensively used in modeling microstructure evolution during phase transformation and its coarsening [14]. Al-Li system with δ' precipitates is considered because of the small lattice mismatch

PII: S1359-6462(00)00323-7

between precipitate and matrix, eliminating the need for considering the effect of elastic energy on coarsening.

Phase-Field Model

In the continuum phase-field model, a two-phase microstructure in a binary system is described by a composition field, $c(\mathbf{r})$, which describes the spatial compositional distribution, and/or a structural order parameter field, $\eta(\mathbf{r})$, which distinguishes the structural difference between the two phases. In the particular example of $\alpha+\delta'$ two-phase microstructure in Al-Li binary alloys, the structural order parameter field is a long-range order parameter which characterizes the structural difference between disordered α matrix and $L1_2$ ordered δ' precipitates. The long-range order parameter has three components, η_1,η_2,η_3 [15]. Therefore, in an $\alpha+\delta'$ two-phase microstructure, the values for all three components of long-range order are zero within the disordered matrix, and the composition field assumes a value close to equilibrium composition of the disordered phase determined by the phase diagram. Within the precipitate particles, three components of the order parameter field have finite values describing the degree of order, and the value of compositional field is close to the equilibrium composition of the δ' ordered phase.

To specify the thermodynamics of $\alpha+\delta'$ two-phase mixture at a given temperature, we employ the following local free energy density function [16,17],

$$f(c,\eta) = \frac{A_1}{2}(c - C_1)^2 + \frac{A_2}{6}(C_2 - c)\sum_{i=1}^{3}\eta_i^2 - \frac{A_3}{3}\prod_{i=1}^{3}\eta_i + \frac{A_4}{24}\sum_{i=1}^{3}\eta_i^4 + \frac{A_5}{24}\sum_{i\neq j}\eta_i^2\eta_j^2 \qquad (1)$$

where C_1 and C_2 are constants close to the equilibrium compositions of α and δ' phases. A_1, A_2, A_3, A_4 and A_5 are positive constants which are functions of composition and temperature. At a constant temperature and composition, the equilibrium value of order parameter can be obtained by minimizing the free energy. The parameters in the free energy model are chosen such that the following sets of combinations for three components of the order parameter provide minimum free energy at a fixed temperature and composition: (η_e, η_e, η_e), $(\eta_e, \bar{\eta}_e, \bar{\eta}_e)$, $(\bar{\eta}_e, \eta_e, \bar{\eta}_e)$, $(\bar{\eta}_e, \bar{\eta}_e, \eta_e)$, where η_e is the equilibrium value of order parameter. These four sets of solutions correspond to four possible translational domains of ordered δ' phase. The free energy of ordered phase as a function of composition is given by $f(c,\eta e_e(c))$ and free energy of disordered phase by $f(c,\eta = 0)$. From the two free energy curves, the equilibrium compositions of two-phase mixture at a given temperature can be obtained by constructing a common tangent. Using the values 0.0571, 0.2192, 125.12, 44.74, 21.21, 22.14 and 22.14 for C_1, C_2, A_1, A_2, A_3, A_4 and A_5, respectively, the equilibrium compositions of α matrix and δ' precipitates are found to be $c_\alpha = 0.0612$ and $c_{\delta'} = 0.24$, respectively.

The interfacial energy between the precipitates and matrix is introduced through the gradient of spatially dependent field variables. At relatively high temperatures at which significant coarsening can take place, interfacial energy anisotropy is small, and hence, it is reasonable to neglect the effect of interfacial energy anisotropy on morphology and coarsening kinetics. Within the diffuse-interface description, the total free energy of an inhomogeneous system with isotropic interfacial energy is given by [18]

$$F = \int \left(f(c,\eta) + \sum_{i=1}^{3}\frac{\beta_i}{2}(\nabla\eta_i)^2 + \frac{\alpha}{2}(\nabla c)^2 \right) dV \qquad (2)$$

where α and β_i are gradient energy coefficients.

The temporal evolution of field variables, hence the microstructure, is obtained by solving Cahn-Hilliard and Allen-Cahn equations [19]. With thermal noise, the equations are

$$\frac{\partial c(\vec{r},t)}{\partial t} = M\nabla^2 \frac{\delta F}{\delta c(\vec{r},t)} + \xi(\vec{r},t) \tag{3}$$

$$\frac{\partial \eta_1(\vec{r},t)}{\partial t} = -L \frac{\delta F}{\delta \eta_i(\vec{r},t)} + \zeta_i(\vec{r},t) \quad ; \quad i = 1,2,3 \tag{4}$$

where $\xi(\vec{r},t)$ and $\zeta_i(\vec{r},t)$ are noise terms which are Gaussian distributed and satisfies the correlation condition [20].

Results and Discussion

In this work, numerical solution of phase-field equations were obtained using semi-implicit Fourier-spectral method in which time variable is discretized using semi-implicit schemes and space variables are discretized using Fourier-spectral method [21]. The noise terms are added to induce sufficiently large fluctuations in composition and long-range order parameter profiles to overcome the nucleation barrier during the initial stages of precipitation. In order to nucleate large number of precipitate particles within a reasonable simulation time, arbitrary large amplitudes are used for noise term, and hence nucleation rates are incorrect. However, since our main focus in the paper is on coarsening kinetics, the rate of nucleation is not critical. In the simulation, noise terms were switched off after initial nucleation.

The system size for 2D and 3D are chosen as 1024^2 and 200^3, respectively, to ensure enough particles at late stages. A mesh size of $\Delta x = 1.0$ is chosen and the volume fraction chosen for study is approximately 20%. The value for Δx is chosen such that interface width is larger compared to the mesh size. If the number of grid points are not sufficient to discretize the interfacial region, particles tend to become anisotropic and take the shape of underlying discrete lattice, and rate of coarsening obtained from numerical simulation is not accurate. Our test showed that $\Delta x = 1.0$ is sufficiently large and any further reduction in Δx yields essentially the same results. For this simulation, α, β_i and Δt are chosen as 0.0, 0.75 and 0.1, respectively. The choice of $\alpha = 0$ is only for convenience since we can still fit the value for β_i to the experimentally measured or fundamentally calculated interfacial energy. The initial condition, which is a super-saturated disordered solid solution, is generated by assigning the overall average composition for the composition field and zero value for the order parameter field at each grid point. The temporal evolution of precipitate morphology and spatial distribution were obtained from the spatial profiles of field variables as a function of time. Statistical data extracted from simulated microstructures were used for analyzing the kinetics of coarsening. The results are obtained by averaging the data from two runs with different initial conditions.

The temporal microstructural evolution during precipitation and coarsening are shown in Figs. 1 and 2 for 2D and 3D, respectively. The number of particles just after nucleation is approximately 4000 and 2200 for 2D and 3D, respectively, and it is approximately 500 and 200 during the final stages. From Figs. 1 and 2, the particle morphologies are similar in both 2D and 3D, except that one is circular and other is spherical.

Since $L1_2$ particles belong to four different types of domains, two neighboring particles may coalesce to one particle or stay separated by disordered matrix. Based on visual inspection of the morphologies in Figs. 1 and 2, coalescence occurs both in two and three dimensions to form dumbbell-shaped particles, but it appears more frequent in 3D than in 2D. Therefore, it is important that any successful coarsening theory should take into account the possibility of coalescence even at relatively low volume fractions. The frequency of coalescence increases with volume fraction [22].

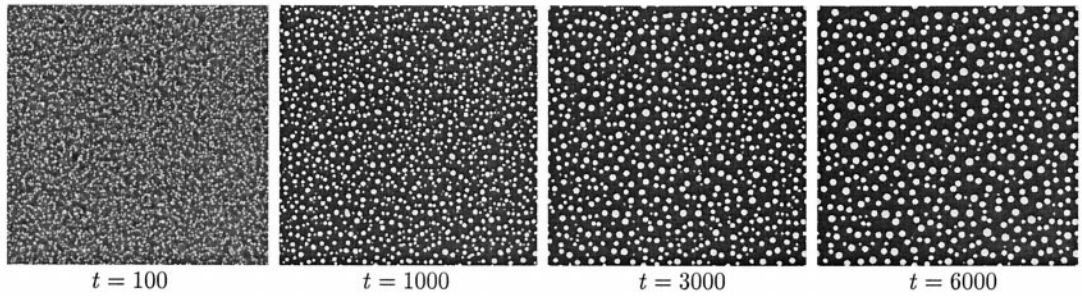

Figure 1. Microstructural evolution from 2D simulation, showing nucleation, growth, and coarsening of δ' (white) particles from an α (black) disordered matrix.

To characterize the average spatial scale of a microstructure and its temporal evolution, we calculated structure function, defined as [7]:

$$S(\mathbf{k},t) = \left\langle \frac{1}{N} \sum_{\mathbf{r}} \sum_{\mathbf{r}'} e^{-i\mathbf{k}.\mathbf{r}} [c(\mathbf{r}' + \mathbf{r},t)c(\mathbf{r}',t) - \langle c \rangle^2] \right\rangle \tag{5}$$

The summations in above equation run over the entire lattice and $N = L^d$, where d is dimensionality of the system (assuming a system with the same linear dimension along all the directions). An inverse Fourier transformation of the structure function gives rise to real-space pair-correlation function. Assuming that the microstructure is statistically isotropic, circularly averaged structure factor (normalized by value of pair correlation function at origin), $s(k,t)$ is defined as:

$$s(k,t) = \frac{\sum_{k-\frac{1}{2}\delta k < |\mathbf{k}| \le k+\frac{1}{2}\delta k} S(\mathbf{k},t)}{[\langle c^2(t) \rangle - \langle c \rangle^2] \sum_{k-\frac{1}{2}\delta k < |\mathbf{k}| \le k+\frac{1}{2}\delta k} 1} \tag{6}$$

Figs. 3(a) and Fig. 3(b) show circularly averaged structure functions plotted at different time steps for 2D and 3D systems, respectively. As time increases, both structure functions become more narrowly distributed and their maximum positions shift to lower k values. k_{max} is proportional to inverse of the average real-space microstructure length scale.

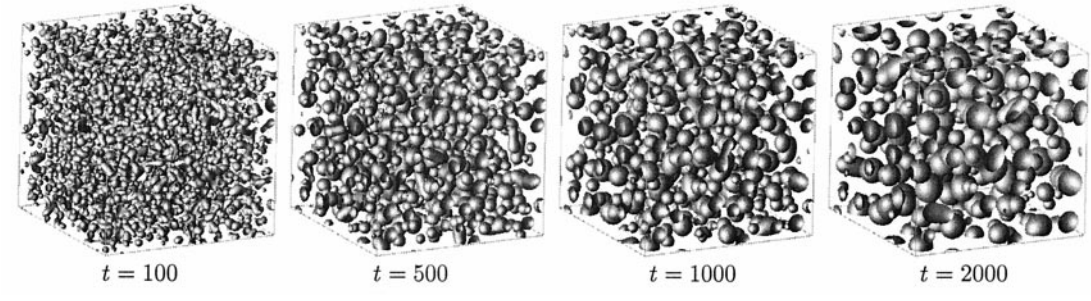

Figure 2. Microstructural evolution from 3D simulation, showing nucleation, growth and coarsening of δ' (gray) particles from an α (transparent) disordered matrix.

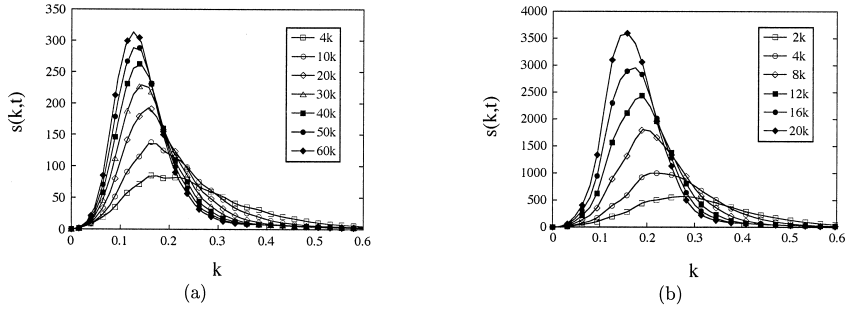

Figure 3. Circularly averaged structure factor vs. k for (a) 1024^2 system at seven different time steps; (b) 200^3 system at six different time steps.

In order to determine whether or not a system has reached the scaling state and to compare 2D and 3D systems, a scaling function, $\mathcal{F}$, is defined based on structure function.

$$\mathcal{F}(k/k_1(t)) = k_1(t)^d \, s(k,t) \tag{7}$$

where d is dimensionality of the system and $k_1(t)$ is the first moment of structure function. A corresponding real-space scaling function based on pair-correlation function is given by

$$\mathcal{G}(r/R_g(t)) = g(r/R_g(t),t) = \frac{\sum_{\mathbf{k}} S(\mathbf{k},t)\, e^{i\mathbf{k}.\mathbf{r}/R_g(t)}}{[\langle c^2(t)\rangle - \langle c\rangle^2]} \tag{8}$$

where $R_g(t)$ is the first zero of pair-correlation function. The Fourier- and real-space scaling functions for both 2D and 3D are shown in Fig. 4a and b, respectively. The Fourier-space scaling functions for both 2D and 3D were normalized such that their maximums are located at $k/k_{max} = 1$. These normalized scaling functions are compared with small angle X-ray scattering results obtained by Che et al [23]. It should be pointed out that although the shapes of scaling functions in 2D and 3D are similar, the maximum values of scaling function in 2D and 3D are totally different. For comparison, we have normalized each set of data in Fig. 4a using their own maximum values. The scaling functions from both 2D and 3D agree reasonably well with experimental results. In Fig. 4b, real-space scaling functions at different times are included for both 2D and 3D. Again, the shapes of scaling functions in 2D and 3D are similar, but the values are different. We also calculated the size of individual precipitates in both

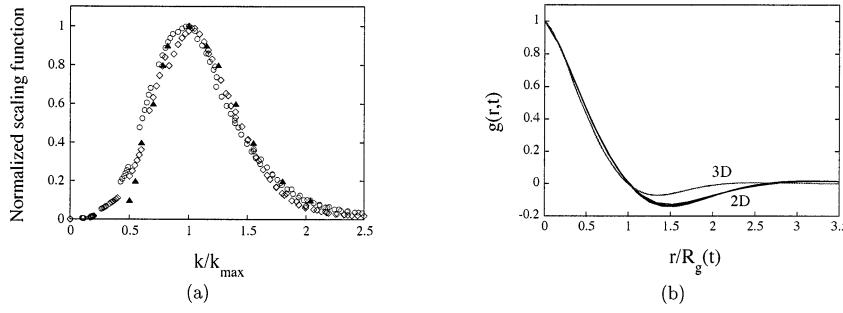

Figure 4. (a) Comparison of normalized 2D and 3D scaling function obtained from $s(k,t)$ with experimental result. Unfilled circles represent 2D, unfilled lozenges represent 3D and filled triangles represent experimental result of Che et al [23] Normalized real space scaling functions in 2D and 3D.

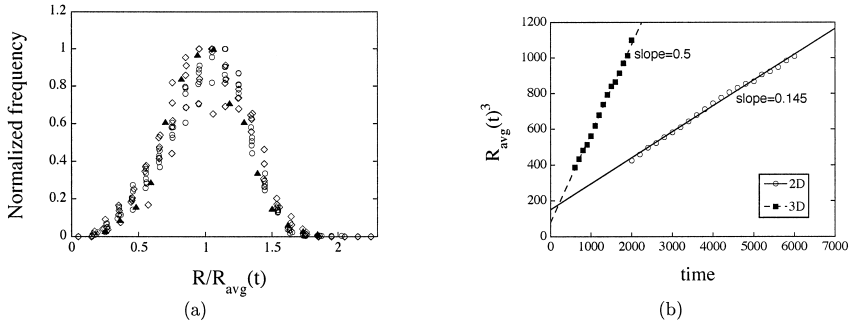

Figure 5. (a) Comparison of late stage NFDs from simulation with experimental result of Gu et Liedl [24]. Unfilled circles represent 2D, unfilled lozenges represent 3D and filled triangles represent experimental result; (b) Comparison of the plots of $R_{avg}(t)^3$ vs. time from 2D and 3D simulation. Slope of the linear fit represents the coarsening rate constant.

2D and 3D at different times. Size in 2D and 3D were obtained from area and volume of the particles, respectively. The normalized particle size distributions (PSDs), which are not included here, exhibits good scaling behavior in both cases during late stages of coarsening. The maximum particle size in both cases is approximately 1.7 times the average particle size. In order to compare simulation results from 2D and 3D with published experimental results, normalized frequency distributions (NFDs) were obtained (normalized frequency here implies that frequency in each interval is divided by the maximum frequency). The experimental result from an Al-Li alloy with ~20% volume fraction δ' by Gu et Liedl [24] is compared with late stage NFDs from simulation in Fig. 5a. The experimental result which was obtained from TEM micrograph of thin foils is in good agreement with the simulation results. The scatter of data is more in 3D compared to 2D because the number of particles in late stages is smaller in 3D.

Finally, most of the coarsening theories predicted that cube of average particle size is a linear function of time at late times. The cubic law was also verified in many experimental measurements and recent computer simulations of coarsening kinetics in two dimensions. The values of $\langle R_{avg}(t)\rangle^3$ are plotted for comparing 2D and 3D growth rates in Fig. 5b. The rate constant in 3D is more than 3 times the value in 2D, indicating that coarsening is significantly faster in 3D than in 2D with same set of thermodynamic and kinetic parameters. The main reason that the size of particles in 3D increases faster than 2D is because of the larger driving force available for coarsening in the form of interfacial curvature.

Conclusion

The coarsening kinetics of δ'-Al_3Li precipitates in a disordered fcc matrix (α) were studied using a continuum diffuse-interface phase-field approach. The $\delta' - \alpha$ two-phase microstructure is described by a three-component order parameter field and a concentration field. The temporal evolution of these fields were obtained by solving the coupled Allen-Cahn and Cahn-Hilliard equations. A 20% precipitate volume fraction was chosen for this study. The emphasis is on the similarities and differences in coarsening kinetics between two and three dimensions (2D and 3D) by examining the morphological evolution and particle growth rates. The cube of average particle size is found to have an approximate linear dependence with time in both 2D and 3D systems. The scaling functions and PSDs obtained in both 2D and 3D exhibited similar approximately time-invariant profiles. The main difference between 2D and 3D systems is in the rate of coarsening for the same set of thermodynamic and kinetic parameters.

Acknowledgments

The authors are grateful for the financial support from the National Science Foundation under DMR96–33719.

References

1. I. M. Lifshitz and V. V. Slyozov, J. Phys. Chem. Solids. 19, 35 (1961).
2. C. Wagner, Z. Elektrochem. 65, 581 (1961).
3. A. J. Ardell, Phase Transformations ’87, p. 485, The Institute of Metals, London (1987).
4. P. W. Voorhees, Annu. Rev. Mater. Sci. 22, 197 (1992).
5. S. P. Marsh and M. E. Glicksman, Acta Mater. 44, 3761 (1996).
6. T. M. Rogers and R. C. Desai, Phys. Rev. B. 39, 4848 (1989).
7. A. Chakrabarti, R. Toral, and J. D. Gunton, Phys. Rev. E. 47, 3025 (1993).
8. N. Akaiwa and D. I. Meiron, Phys. Rev. E. 54, R13 (1996).
9. T. Kupper and N. Masbaum, Acta Mater. 42, 1847 (1994).
10. A. Chakrabarti, R. Toral, and J. D. Gunton, Phys. Rev. B. 39, 4386 (1989).
11. J. H. Yao, K. R. Elder, H. Guo, and M. Grant, Phys. Rev. B. 47, 14110 (1993).
12. N. Akaiwa and P. W. Voorhees, Phys. Rev. E. 49, 3860 (1994).
13. R. Poduri and L. Q. Chen, Acta Mater. 46, 3915 (1998).
14. L. Q. Chen and Y. Wang, JOM. 48, 13 (1996).
15. Z. W. Lai, Phys. Rev. B. 41, 9239 (1990).
16. D. Y. Li and L. Q. Chen, Scripta Mater. 37, 1271 (1997).
17. Y. Wang, D. Banerjee, C. C. Su, and A. G. Khachaturyan, Acta Mater. 46, 2983 (1998).
18. J. W. Cahn and J. E. Hillard, J. Chem. Phys. 28, 258 (1958).
19. S. M. Allen and J. W. Cahn, Acta Metall. 27, 1084 (1979).
20. K. Elder, Computers Phys. 7, 27 (1993).
21. L. Q. Chen and J. Shen, Comp. Phys. Commun. 108, 147 (1998).
22. D. J. Chellman and A. J. Ardell, Acta Metall. 22, 577 (1974).
23. D. Z. Che, S. Spooner, and J. J. Hoyt, Acta Mater. 45, 1167 (1997).
24. B. P. Gu and G. L. Liedl, Mater. Sci. Eng. 70, 217 (1985).